

1 **Damage-induced pyroptosis drives endogenous thymic regeneration via**  
2 **induction of Foxn1 by purinergic receptor activation**  
3 Sinéad Kinsella<sup>1,2</sup>, Cindy A. Evandy<sup>1,2</sup>, Kirsten Cooper<sup>1,2</sup>, Antonella Cardinale<sup>3</sup>, Lorenzo Iovino<sup>1,2</sup>,  
4 Paul deRoos<sup>1,2</sup>, Kayla S. Hopwo<sup>1,2</sup>, Colton W. Smith<sup>1,2</sup>, David Granadier<sup>1,2,4</sup>, Lucas B. Sullivan<sup>5</sup>,  
5 Enrico Velardi<sup>3</sup> and Jarrod A. Dudakov<sup>1,2,6</sup>

6

7 <sup>1</sup>Program in Immunology, Division of Translational Science and Therapeutics, Fred Hutchinson  
8 Cancer Center, Seattle WA, 98109, US

9 <sup>2</sup>Immunotherapy Integrated Research Center, Fred Hutchinson Cancer Research Center,  
10 Seattle WA, 98109, US

11 <sup>3</sup>Department of Pediatric Hematology and Oncology, Bambino Gesù Children's Hospital,  
12 IRCCS, Rome, 00146, Italy

13 <sup>4</sup>Medical Scientist Training Program, University of Washington, Seattle WA, 98195, US

14 <sup>5</sup>Human Biology Division, Fred Hutchinson Cancer Center, Seattle WA, 98109, US

15 <sup>6</sup>Department of Immunology, University of Washington, Seattle WA, 98195, US

16

17 **SUMMARY:**

18     • Thymocytes rapidly and transiently undergo pyroptosis after acute thymic damage and  
19        promote regeneration.

20     • Damage-induced redirection of pyruvate acutely enhances mitochondrial OXPHOS in  
21        thymocytes.

22     • Elevated mitochondrial ROS promotes pyroptosis in thymocytes after acute insult by  
23        driving caspase 1 cleavage.

24     • Extracellular ATP release promotes *Foxn1* expression in cTECs via activation of P2Y2

25     • Therapeutic targeting of the P2Y2 receptor promotes thymic regeneration.

26 **ABSTRACT**

27 Endogenous thymic regeneration is a crucial process that allows for the renewal of immune  
28 competence following stress, infection or cytoreductive conditioning. Fully understanding the  
29 molecular mechanisms driving regeneration will uncover therapeutic targets to enhance  
30 regeneration. We previously demonstrated that high levels of homeostatic apoptosis suppress  
31 regeneration and that a reduction in the presence of damage-induced apoptotic thymocytes  
32 facilitates regeneration. Here we identified that cell-specific metabolic remodeling after ionizing  
33 radiation steers thymocytes towards mitochondrial-driven pyroptotic cell death. We further  
34 identified that a key damage-associated molecular pattern (DAMP), ATP, stimulates the cell  
35 surface purinergic receptor P2Y2 on cortical thymic epithelial cells (cTECs) acutely after damage,  
36 enhancing expression of *Foxn1*, the critical thymic transcription factor. Targeting the P2Y2  
37 receptor with the agonist UTPyS promotes rapid regeneration of the thymus *in vivo* following acute  
38 damage. Together these data demonstrate that intrinsic metabolic regulation of pyruvate  
39 processing is a critical process driving thymus repair and identifies the P2Y2 receptor as a novel  
40 molecular therapeutic target to enhance thymus regeneration.

41

42

43

44

45

46

47

48

49 **KEY WORDS:** Thymus regeneration, cell death, pyroptosis, pyruvate, mitochondria, ATP,  
50 DAMPs, purinergic receptors, P2Y2

51

52 **INTRODUCTION**

53 Competent T cell development relies on efficient functioning of the thymus, which is extremely  
54 sensitive to acute insults, such as that caused by cytoreductive therapies<sup>1</sup>. Thymic function  
55 progressively declines with age, resulting in reduced export of newly generated naïve T cells and  
56 reduced responsiveness to new antigens and vaccines<sup>2, 3</sup>. The thymus has a remarkable ability  
57 to endogenously regenerate<sup>4, 5, 6</sup>, however, age-related deterioration drastically erodes this  
58 regenerative capacity<sup>7</sup>. Harnessing this regenerative capacity has the potential to expedite  
59 reconstitution of naïve T cells and improve immune responses. However, much remains unknown  
60 about the molecular regulators of this critical process.

61

62 We have previously identified that IL-22 and BMP4 represent two distinct pathways that facilitate  
63 endogenous repair in the thymus and, at least in the case of BMP4, is largely mediated by  
64 induction in the expression of Foxn1<sup>5, 8</sup>. FOXN1 is the essential thymic epithelial cell (TEC)  
65 transcription factor; not only crucial for the generation and function of TECs, but also for TEC  
66 maintenance with declining expression associated with age-related thymic involution<sup>9</sup>. We have  
67 previously identified that the constitutively high levels of homeostatic apoptosis in the steady state  
68 thymus, which governs negative selection events, is suppressive to the production of BMP4 and  
69 IL-23 (the upstream regulator of IL-22), and the depletion of apoptotic thymocytes after injury  
70 promotes their production<sup>10</sup>. Cell death is a sophisticated and tightly controlled process and much  
71 of this is regulated by the mitochondria, and notably necrotic cell death has been tightly linked to  
72 regeneration<sup>11, 12, 13, 14, 15, 16</sup>.

73

74 Given the robust depletion of thymocytes after acute damage concurrent to the activation of these  
75 reparative pathways, we hypothesized that a switch to an alternative cell death mechanism may  
76 underpin the triggering of tissue regeneration and alleviate the suppressive impact of apoptosis  
77 in the thymus. Here we investigated the effects of acute damage on the metabolic landscape of

78 thymocytes and revealed that increased levels of pyruvate are redirected to mitochondrial  
79 respiration, reducing glycolysis. This disrupted glycolytic flux drives pyroptosis in the thymus  
80 which is rapidly resolved as regeneration begins.

81  
82 These findings identify a novel mechanism of metabolic regulation of T cell development and  
83 thymic repair and provides a highly targetable therapeutic strategy to enhance immune function.

84  
85 **RESULTS**

86 ***DP thymocytes preferentially undergo pyroptosis after damage***

87 Most thymocytes, and in particular CD4+CD8+ double positive (DP) thymocytes, undergo  
88 apoptosis as a function of the selection processes fundamental to T cell development<sup>17, 18</sup>. We  
89 previously identified that homeostatic detection of these apoptotic events suppresses the  
90 production of multiple regenerative molecules in the thymus by promoting activation of TAM  
91 receptors bridging phosphatidylserine (PtdSer) sensing by surrounding stromal cells<sup>10</sup>. However,  
92 although we had previously found that after acute damage there is a rapid decrease in the  
93 detection of PtdSer<sup>10</sup>, this declined more rapidly than cell depletion itself (**Fig. 1A**) which led us  
94 to hypothesize that alternate forms of cell death may be being induced after acute damage. Given  
95 that DP thymocytes are the most numerous, comprising ~80% of a thymus at baseline, and these  
96 cells are extremely sensitive to damage and are depleted rapidly after sub-lethal total body  
97 irradiation (TBI, 550 cGy) (**Fig. 1B**), we concentrated on this population. Not surprisingly we did  
98 find considerable cleavage of caspase-3 (executioner apoptosis caspase) within thymocytes (**Fig.**  
99 **1C**), consistent with previous reports demonstrating their sensitivity to damage<sup>19, 20</sup>. However, we  
100 also found significant cleavage of caspase-1 in dying cells suggesting that in addition to  
101 immunologically silent apoptosis, there is also considerable pyroptosis occurring amongst  
102 thymocytes after acute injury caused by TBI (**Fig. 1D**). In fact, direct comparison revealed similar  
103 magnitude of activation of both caspase-3 and caspase-1 after damage in DP thymocyte (**Fig.**

104 **1E**). Consistent with this induction of immunogenic form of cell death, we found increased release  
105 of lactate dehydrogenase in the thymus after TBI (**Fig. 1F**) as well as increased levels of  
106 gasdermin D (**Fig. 1G**), all suggesting a preferential induction of pyroptosis following acute  
107 damage.

108  
109 Since apoptosis is largely suppressive tissue regeneration in the thymus<sup>10</sup>, we hypothesized that  
110 lytic cell death of DPs may be beneficial to regeneration. Moreover, as thymocyte depletion  
111 precedes the period of epithelial regeneration largely driven by enhanced *Foxn1* transcription<sup>21</sup>,  
112 we tested if pyroptotic thymocytes could directly influence *Foxn1* expression in TECs. To do this  
113 we induced pyroptosis in freshly isolated thymocytes *ex vivo* using Nigericin and LPS and co-  
114 cultured the dying cells with cortical thymic epithelial cells (cTECs, using the 1C9 and ANV42.1  
115 cell lines) and medullary thymic epithelial cells (mTEC, using the TE-71 cell line) and quantified  
116 *Foxn1* expression (**Fig. 1H**). Using this approach, we could demonstrate that the presence of  
117 pyroptotic thymocytes directly led to upregulation of *Foxn1* transcription in cTECs but not in  
118 mTECs (**Fig. 1H**). This cell-specific regulation of *Foxn1* was notable given that we have previously  
119 shown that *Foxn1* upregulation during endogenous regeneration after damage is largely restricted  
120 to cTECs<sup>8</sup>.

121  
122 ***Mitochondrial dysregulation facilitates pyroptosis in DPs***  
123 In addition to the critical role of mitochondria in cellular metabolism, the mitochondria is a  
124 gatekeeper of cell death and dysregulated mitochondrial bioenergetics can lead to the induction  
125 of intrinsic apoptosis or pyroptosis<sup>22, 23, 24, 25</sup>. As thymocytes are undergoing such high levels of  
126 homeostatic cell death we sought to understand if metabolic adaptations were steering cell death  
127 preferences after damage. First, measuring mitochondrial membrane potential using TMRE  
128 revealed a marked induction of mitochondrial membrane hyperpolarization (**Fig. 2A**), correlating  
129 to increased cleaved caspase 1 (cl-caspase 1) levels (**Fig. 2B**). Importantly, this enhanced

130 mitochondrial activation was resolved by day 7 following damage, in line with what we observed  
131 with caspase 1 cleavage and the re-establishment of apoptosis:pyroptosis balance (**Fig. 1E**).  
132 Additional evidence of an acute damage-induced dysregulated metabolic phenotype in DPs was  
133 revealed with increased mitochondrial mass in DPs after acute damage, which could also be  
134 positively correlated with Cas1 activation (**Fig. 2C-D**).

135

136 ***Increased mitochondrial ROS triggers pyroptosis in thymocytes***

137 Bidirectional communication between the mitochondria and the NLRP3 inflammasome has been  
138 well characterized and can induce activation of NLRP3 signaling<sup>26, 27, 28</sup>, while concurrently  
139 facilitating a lack of mitophagy driven by cleavage of caspase 1<sup>29, 30</sup>. This positive feedback loop  
140 perpetuates the accumulation of ROS-producing dysfunctional mitochondria due to a lack of  
141 mitophagy, which in turns continues to initiate NLRP3-induced pyroptotic cell death<sup>25, 31</sup>. Next, we  
142 hypothesized that transiently enhanced mitochondrial activation in DPs led to increased  
143 production of mitochondrial ROS (mitoROS) providing a trigger for pyroptosis. Consistent with  
144 mitochondrial hyperpolarization, mitochondrial mass and cl-caspase 1 levels, there was a  
145 transient and precipitous elevation in mitoROS levels after damage, again correlating with  
146 caspase-1 cleavage (**Fig. 2E-F**). This increase in mitoROS was coupled with a robust and acute  
147 induction in glutathione levels (**Fig. S1**), suggesting antioxidant pathways are upregulated. RNA  
148 seq analysis of DP thymocytes at baseline and 24 hours after TBI revealed an increase in *Ucp2*  
149 and *Mitofusin 2* (**Fig 2G**), which are central facilitators of proton leakage and Nlrp3 activation<sup>32, 33</sup>.  
150 RNA sequencing on DP thymocytes also revealed an enrichment for genes regulating OXPHOS  
151 (*Igf2bp2*, *Ybx1*, *Ucp2*) and, importantly, downregulation of pyruvate processing to lactate (*Ldhb*),  
152 pointing to a redirection of pyruvate to fuel OXPHOS (**Fig. 2G**). Of note, genes encoding key  
153 glycolysis enzymes, such as *Hk1* and *Hk2*, were upregulated after TBI suggesting an increase in  
154 glucose uptake, providing increased levels of pyruvate as fuel for mitochondrial metabolism<sup>34, 35</sup>.  
155

156 In order to demonstrate that dysregulated metabolism was driving this shift from apoptosis to  
157 pyroptosis after damage, we examined the role of increased mitochondrial metabolism on cell  
158 death in thymocytes. Firstly, to assess any damage-induced alterations in glycolytic flux we  
159 measured pyruvate and lactate levels in thymocytes at rest and 24 h after damage and the ratio  
160 of pyruvate to lactate was significantly increased early after damage (**Fig. 2H**); strengthening our  
161 findings of a damage-induced metabolic shift away from glycolysis and towards OXPHOS. Next,  
162 to determine if enhancing mitochondrial respiration by increasing pyruvate could induce caspase  
163 1 cleavage and cell death, we incubated freshly isolated thymocytes *ex vivo* with high levels of  
164 pyruvate (5 mM). This approach demonstrated that pyruvate induced caspase 1 cleavage in  
165 thymocytes, but this could not be induced in thymocytes isolated from mice given TBI (**Fig. 2I-J**),  
166 suggesting a zenith of pyroptosis, possibly due to the saturation of pyruvate and mitochondrial  
167 activity acutely after damage. Consistent with this proposed mechanism, treatment of thymocytes  
168 with high levels of pyruvate strongly induced mitoROS (**Fig. 2K**) and targeting mitoROS with the  
169 inhibitor TEMPOL reduced cl-caspase 1 levels in thymocytes under pyruvate pressure (**Fig. 2L**).  
170 Finally, blocking pyruvate conversion to acetyl co-A with  $\alpha$ -ketobutyrate ( $\alpha$ -KB) reduced cl-  
171 caspase 1 levels, demonstrating a role of the TCA cycle in pyroptosis induction in thymocytes  
172 (**Fig. 2M**). These findings were consistent with a demonstration that fueling increased proton  
173 leakage and increased mitoROS triggers pyroptosis in thymocytes after damage, confirming DPs  
174 preferentially undergo pyroptotic cell death after damage facilitated by increased pyruvate-  
175 induced production of mitoROS.

176

### 177 ***Extracellular ATP induces Foxn1 expression in cTECs***

178 Pyroptotic cell death produces a plethora of molecules that act as ligands and messengers to  
179 facilitate communication with neighboring cells<sup>36,37,38</sup>. We have previously shown that extracellular  
180  $Zn^{2+}$  can act as a damage-associated molecular pattern (DAMP) after acute damage, inducing  
181 expression of the pro-regenerative molecule BMP4 in endothelial cells via the receptor GPR39<sup>39</sup>.

182 However, activation of GPR39 on TECs failed to induce *Foxn1* expression. We thus sought to  
183 identify specific DAMPs that could trigger the induction of *Foxn1* transcription, specifically  
184 focusing on cTECs. To this end, we tested the response of the cTEC cell line (1C9) to a panel of  
185 DAMPs and identified ATP to be a strong inducer of *Foxn1* transcription (**Fig. 3A**). This finding  
186 was confirmed in another cTEC cell line (ANV42.1) (**Fig. 3B**) and, importantly, freshly isolated  
187 human TECs (**Fig. 3C**).

188

189 ATP is a ligand for cell surface purinergic receptors and can activate downstream signaling  
190 pathways that either induce the influx of extracellular  $\text{Ca}^{2+}$  or promote the efflux of ER  $\text{Ca}^{2+}$  via G-  
191 coupled signaling<sup>40, 41, 42</sup>. Previous studies have found that purinergic receptor expression is  
192 heterogeneous between thymic epithelial cell subsets, with widespread expression of both P2Y  
193 and P2X receptors expressed among all subsets of TECs<sup>43</sup>. Consistent with this, specific analysis  
194 of TEC subsets by RNA sequencing revealed expression of multiple P2X and P2Y receptors  
195 across cTECs and mTECs, with expression on cTECs limited to *P2rx1*, *P2rx4*, *P2rx6*, *P2rx7*,  
196 *P2ry1*, *P2ry2*, and *P2ry14* (**Fig. 3D**). Baseline expression levels of purinergic receptors were  
197 confirmed by qPCR on the 1C9 (cTEC cell line), and on freshly isolated murine cTECs (**Fig. 3E**).  
198 Next, as P2 receptor activation induces a downstream increase in intracellular  $\text{Ca}^{2+}$  levels, we  
199 measured  $\text{Ca}^{2+}$  levels in cTECs and mTECs after damage and demonstrated an increase in  $\text{Ca}^{2+}$   
200 in cTECs but not mTECs (**Fig. 3F**), with positive correlation between  $\text{Ca}^{2+}$  levels with *Foxn1*  
201 expression (**Fig. 3G**). This data is consistent with the cell-specific effects of pyroptotic thymocytes  
202 on *Foxn1* expression in cTECs, suggesting cTECs are central gatekeepers of the ATP-mediated  
203 regenerative response. As P2X and P2Y receptor activation regulate  $\text{Ca}^{2+}$  levels differently<sup>40</sup>, we  
204 assessed the effect of ATP on both  $\text{Ca}^{2+}$  influx and efflux within cTECs. To do this we treated  
205 cTECs with tunicamycin, to induce ER release of  $\text{Ca}^{2+}$  into the cytosol, or thapsigargin, to inhibit  
206 ER  $\text{Ca}^{2+}$  release, and revealed that flooding the cell with  $\text{Ca}^{2+}$  led to enhanced *Foxn1* expression,  
207 while attenuating  $\text{Ca}^{2+}$  levels restored *Foxn1* expression to baseline (**Fig. 3H**). These results

208 strongly suggested the role of P2Y receptors in mediating the FOXN1 promoting effects of  
209 extracellular ATP, however, we further sought to refine our target and identify which P2 receptor  
210 was critical to mediate this effect. To confirm this, we treated cTECs with ATP in the presence of  
211 antagonists for P2Y2, and P2X4, as P2X4 is highly expressed on cTECs although does not induce  
212  $\text{Ca}^{2+}$  efflux and demonstrated that inhibition of P2Y2 attenuated ATP-mediated *Foxn1* induction,  
213 mirroring the effects ATP elicits as an extracellular DAMP after acute insult (**Fig. 3I**).

214

215 ***Specific activation of P2Y2 receptors can enhance Foxn1 expression and boost thymic***  
216 ***function after acute injury***

217 P2 antagonists are of increasing interest therapeutically, with a focus on developing analogous  
218 molecules to inhibit or promote these druggable targets in many disease settings, such as  
219 epilepsy<sup>44</sup>, rheumatoid arthritis<sup>45</sup> and ischemic cardiac injury<sup>46</sup>. Moreover, clinical trials have been  
220 carried out using antagonists for P2X3<sup>47</sup>, P2X7<sup>48,49</sup> and P2Y12<sup>50</sup>. To test if P2Y2 could be targeted  
221 to enhance FOXN1 we obtained a specific P2Y2 agonist and further demonstrated that stimulation  
222 of cTECs with a P2Y2 agonist induced *Foxn1* expression, and inhibition of P2Y2 ablated this  
223 response (**Fig. 4A**). We sought to translate our molecular target discovery findings into a  
224 therapeutic strategy *in vivo* to test if P2Y2 agonism could enhance thymic regeneration. To do  
225 this we treated C57BL/6 mice with SL-TBI and administered the P2Y2 agonist UTP $\gamma$ S  
226 intraperitoneally at day 1 following damage and assessed thymic cellularity 13 days after damage  
227 and confirmed that UTP $\gamma$ S could enhance thymus regeneration after acute damage (**Fig. 4B**).  
228 Additionally, *in vivo* treatment with UTP $\gamma$ S had a global impact on thymocyte populations, with  
229 increased regeneration of DPs, CD4+ and CD8+ thymocytes and superior regeneration of the  
230 TEC compartment (**Fig. 4C**).

231

232

233

234 **DISCUSSION**

235 Endogenous thymic regeneration engages complex multicellular signaling networks that  
236 intricately communicate within cellular niches to repair and replenish peripheral T cell  
237 reconstitution. Here, we demonstrated that an induction of pyroptosis as a preferred cell death  
238 mechanism provides the critical ligand ATP, that stimulated P2Y2 receptors on cTECs to promote  
239 FOXN1 transcription and enhance regeneration of the thymus. Moreover, we uncovered a cell  
240 specific mechanism of metabolically regulated thymus regeneration that is centered on steering  
241 pyruvate processing to induce lytic cell death by dysregulating mitochondrial metabolism, acutely  
242 increasing mitoROS and triggering NLRP3 activation and pyroptosis. Here we identified the  
243 effects of acute damage on the thymocyte metabolic landscape and cell fate.

244

245 The thymus is highly hypoxic<sup>51, 52</sup>, and thymocytes undergo dynamic alterations in respiration  
246 during development (specifically between DN and DP stages)<sup>53</sup>, pointing to their metabolic  
247 plasticity. Here we identified the effects of acute damage on the metabolic landscape of  
248 thymocytes and revealed that increased levels of pyruvate are redirected toward mitochondrial  
249 respiration, reducing glycolysis. Disruption of glycolytic flux has been shown to trigger  
250 pyroptosis<sup>54</sup>, and our data demonstrates that an acutely altered metabolic profile in DP  
251 thymocytes drives pyroptosis in the thymus and is rapidly resolved as regeneration is initiated.  
252 Accompanying damage-induced acute hyperpolarization of the mitochondrial membrane,  
253 increased mitochondrial mass and mitochondrial ROS in DP thymocytes, our RNA sequencing  
254 data showed an upregulation of genes encoding UCP2 and PARP1, key negative regulators of  
255 oxidative stress<sup>55, 56</sup>, and in Mitofusin 2 which governs mitochondrial integrity<sup>57</sup>. Importantly, our  
256 gene signature of damage in DP thymocytes revealed that several genes encoding enzymes  
257 critical for glucose processing to pyruvate, such as HK1, HK2, PKM and HIF1 $\alpha$  were upregulated  
258 concurrently with a downregulation in genes regulating pyruvate conversion to lactate (*Ldhb*).  
259 Functionally resulting in a higher pyruvate to lactate ratio, and redirection towards mitochondrial

260 respiration. ROS reacts with the NLRP3 inflammasome and drives pyroptotic cell death<sup>25, 58, 59, 60,</sup>  
261 <sup>61, 62</sup>. Here we confirmed this in the thymus and demonstrated that pyruvate drives this increase  
262 in mitochondrial ROS that further triggers caspase-1 cleavage and pyroptosis, strengthening the  
263 case for a central role in redirection away from glycolysis as a trigger from thymocyte cell death.

264

265 Both intracellular and extracellular ATP has been previously identified to play a role in tissue  
266 repair<sup>63, 64, 65</sup>, and importantly purinergic receptors are identified to mediate the extracellular ATP  
267 response<sup>66</sup>, with interest in pharmacologically targeting these receptors to enhance wound  
268 repair<sup>67, 68</sup>. Activation of purinergic receptors mobilizes intracellular  $\text{Ca}^{2+}$  in epithelial cells<sup>69</sup>. Here  
269 we identified that inhibiting  $\text{Ca}^{2+}$  efflux from the ER, using thapsigargin, downstream of ATP  
270 treatment prevented FOXN1 transcription, which led us to further assess P2Y2 as a specific  
271 target. Moreover, P2Y2 has been identified to mediate migration and repair of epithelial cells<sup>70</sup>.  
272 Purinergic receptors have been trialed for a range of diseases, for example P2X7 antagonists are  
273 being tested is a Phase 2a clinical trial to treat Crohns disease, while targeting P2X7 to treat  
274 rheumatoid arthritis failed to show significance in phase 2 clinical trial<sup>71</sup>, and the P2Y2 agonist  
275 Diquafosol is currently being tested for the treatment of dry eye<sup>72</sup>. We identified that P2Y2  
276 agonism promotes FOXN1 transcription specifically in cTECs and that competition with an  
277 antagonist quenches this effect, pointing to receptor specificity. Moreover, our pre-clinical data  
278 demonstrates that the P2Y2 agonist UTPyS promotes superior regeneration in acutely injured  
279 mice, promoting recovery of thymocyte and both cTEC and mTEC compartments, which is vital  
280 for continued maintenance and functioning of the thymus.

281

282 While much remains to be understood regarding mitochondrial regulation of cell death and  
283 differentiation in models of chronic damage such as age, these data underline an important  
284 mechanism of recovery from acute damage that highlights the significance of metabolic  
285 governance of immune function. The question of other fuel sources that drive mitochondrial

286 dysfunction during acute damage, such as lipids or glutamine, is outstanding and may potentially  
287 reveal disease specific damage-responses of the thymus, specifically as lipid metabolism has  
288 been identified to play a central role in hematopoiesis and T cell differentiation<sup>73</sup>. However, as  
289 these metabolic phenotypes are likely to be variable between cellular compartments, and with our  
290 data clearly demonstrating a central role of pyruvate in mitochondrial induced pyroptosis, the  
291 convergence of these pathways on mitochondrial ROS is central to pyroptotic driven regeneration.  
292 In conclusion, these data describe a complex molecular architecture that govern thymus  
293 regeneration and not only provides a platform for therapeutic target discovery and intervention  
294 towards enhancing immune function, but also contributes to regenerative medicine by unravelling  
295 novel mechanisms of metabolically regulated endogenous tissue regeneration which may be  
296 applicable across multiple tissues.

297

## 298 **MATERIALS AND METHODS**

### 299 ***Mice***

300 Inbred male and female C57BL/6J mice were obtained from the Jackson Laboratories (Bar  
301 Harbor, USA) and all experimental mice were used between 6-8 weeks old. To induce thymic  
302 damage, mice were given sub-lethal total body irradiation (SL-TBI) at a dose of 550 cGy from a  
303 cesium source mouse irradiator (Mark I series 30JL Shepherd irradiator) with no hematopoietic  
304 rescue. Mice were maintained at the Fred Hutchinson Cancer Research Center (Seattle, WA),  
305 and acclimatized for at least 2 days before experimentation, which was performed per Institutional  
306 Animal Care and Use Committee guidelines.

307

### 308 ***Reagents***

309 Cells were stained with the following antibodies for analysis CD3-FITC (35-0031, Tonbo  
310 Bioscience), CD8-BV711 (100748, BioLegend), CD4-BV650 (100546, BioLegend), CD45-  
311 BUV395 (565967, BD Biosciences), CD90-BV785 (105331, BioLegend), MHC-II-Pac Blue

312 (107620, BioLegend), EpCAM-PercPe710 (46-5791-82, eBioscience), Ly51-PE (12-5891-83,  
313 eBioscience), UEA1-FITC (FL-1061, Vector Laboratories), TCRbeta-PECy7 (109222,  
314 BioLegend), CD62L-APC-Cy7 (104427, BioLegend), CD44-Alexa Fluor RTM700 (56-0441-82,  
315 BioLegend), CD25-PercP-Cy5.5 (102030, BioLegend). Flow cytometry analysis was performed  
316 on an LSRFortessa X50 (BD Biosciences) and cells were sorted on an Aria II (BD Biosciences)  
317 using FACSDiva (BD Biosciences) or FlowJo (Treestar Software).

318

319 ***Thymus digestion and cell isolation***

320 Single cell suspensions of freshly dissected thymuses were obtained and either mechanically  
321 suspended or enzymatically digested as previously described<sup>5, 74</sup> and counted using the Z2  
322 Coulter Particle and Size Analyzer (Beckman Coulter, USA). For studies sorting rare populations  
323 of cells in the thymus, multiple identically treated thymuses were pooled so that sufficient number  
324 of cells could be isolated; however, in this instance separate pools of cells were established to  
325 maintain individual samples as biological replicates.

326

327 ***Cell death assays***

328 Thymuses from untreated and SL-TBI treated mice were harvested, enzymatically digested and  
329 stained with cell surface markers for thymus populations. Cells were further stained for caspase  
330 1 cleavage with Caspase-1 (active) Staining Kit (Abcam, ab219935), or fixed for caspase 3  
331 analysis using Cleaved Caspase-3 (Asp175) Antibody (Alexa Fluor® 488 Conjugate) (Cell  
332 signaling, 9669S). Apoptosis and pyroptosis was assessed by adding Annexin V-FITC  
333 (Biolegend, 640906), Annexin V binding buffer (BioLegend, 422201) and Propidium Iodide  
334 (Invitrogen, BMS500PI). Gasdermin D was measured in freshly isolated thymocytes using  
335 Gasdermin D (mouse) ELISA Kit (Adipogen Life Sciences, AG-45B-0011-KI01). Lactate  
336 dehydrogenase was assessed from the supernatant of harvested thymocytes using Lactate  
337 Dehydrogenase assay (Abcam, ab102526).

338

339 ***In vitro assays***

340 *Co-culture assays*: thymocytes were isolated from untreated C57BL/6 mice and incubated with  
341 Nigericin (10  $\mu$ M, Tocris, 4312) and LPS (1 ng/ml, Invivogen, tlrl-eblps) for 3 h and co-cultured  
342 with 1C9s, ANV42.1 or TE-71 cell lines for 20 h before lysis for qPCR. *DAMP stimulation*: 1C9s  
343 were stimulated with ATP (100  $\mu$ M, Tocris 3312), HMGB1 (1  $\mu$ g/ml, Abcam, ab78940), IL1a (50  
344 ng/ml, Tocris, 400-ML-005/CF), IL-33 (50 ng/ml, Tocris, 3626-ML-010/CF), or uric acid (50  $\mu$ g/ml,  
345 Sigma, U2625) for 20 h and lysed for qPCR analysis. *UTPyS assays*: 1C9s or ANV42, cells were  
346 stimulated with UTPyS (100  $\mu$ M, R&D Systems, 3279), or UTPyS plus AR-C 118925XX (20  $\mu$ M,  
347 Tocris, 4890) for 20 h before lysis for qPCR. BzATP triethylammonium salt (100-300  $\mu$ M, Tocris,  
348 3312), was used for ATP stimulation.

349

350 ***qPCR and RNA sequencing***

351 RNA was extracted from exECs or DCs using a RNeasy Mini kit (74104, Qiagen), and from sorted  
352 cells using a RNeasy Plus Micro kit (74034, Qiagen). cDNA was synthesized using the iScript  
353 gDNA Clear cDNA Synthesis kit (1725035, Bio-Rad, USA) and a Bio-Rad C1000 Touch  
354 ThermoCycler (Bio-Rad). RNA expression was assessed in the Bio-Rad CFX96 Real Time  
355 System (Bio-Rad), using iTaq Universal SYBR Green Supermix (1725122, Bio-Rad), and the  
356 following primers:  $\beta$ -Actin (F 5'-CACTGTCGAGTCGCGTCC-3'; R 5'-  
357 TCATCCATGGCGAACTGGTG-3'); PrimePCR™ SYBR® Green Assay: Foxn1, Mouse (Biorad,  
358 10025637, qMmuCED0044924).

359

360 RNAseq was performed on freshly isolated and FACS purified CD4+CD8+ thymocytes. To obtain  
361 sufficient RNA for every timepoint, thymi of 2 mice were pooled for untreated mice and 6 for  
362 irradiated mice. All samples underwent a quality control on a bioanalyzer to exclude degradation  
363 of RNA.

364

365 ***Ex vivo metabolic assays***

366 Thymuses from untreated and SL-TBI treated mice were harvested and enzymatically digested  
367 and stained from flow cytometry analysis of thymocyte populations as above. Further analysis of  
368 mitochondrial bioenergetics were assessed using TMRE (Abcam, ab113852), MitoTracker™  
369 Green FM (Invitrogen, M7514), MitoSOX™ Red Mitochondrial Superoxide Indicator  
370 (ThermoFisher, M36008), and Intracellular glutathione (GSH) Detection Assay Kit (Abcam,  
371 ab112132). Thymocytes were isolated from untreated and TBI-treated mice and intracellular  
372 pyruvate and lactate levels were measured by absorbance using Pyruvate Assay kit (Abcam,  
373 ab65342) or Lactate-Glo™ Assay (Promega, J5021). Thymocytes were isolated from untreated  
374 and TBI-treated mice and incubated in RPMI with 5 mM sodium pyruvate (Gibco, 11360070) for  
375 3 h at 37 °C and stained for flow cytometry analysis and cl-caspase 1 levels. Cells were further  
376 incubated with 5 mM sodium pyruvate plus 200 µM  $\alpha$ -ketobutyrate (Sigma-Aldrich) or 100 µM  
377 TEMPOL (Tocris, 3082) for 3 h and cells were prepared for flow cytometry analysis.

378

379 ***Intracellular Ca<sup>2+</sup> assay***

380 The thymuses from untreated and SL-TBI-treated mice were harvested and processed for flow  
381 cytometry as above. The intracellular Ca<sup>2+</sup> dye BAPTA-AM/Indo-AM was added (Sigma-Aldrich).  
382 Unbound intracellular Ca<sup>2+</sup> was assessed in cTECs and mTECs by measuring BAPTA-AM levels  
383 on the BUV-496 filter.

384

385 ***In vivo UTPyS administration***

386 For *in vivo* studies of UTPyS administration, mice were given SL-TBI (550cGy) and subsequently  
387 received intraperitoneal injections of 1 mg/kg UTPyS (R&D systems, 3279), or 1x PBS as control,  
388 on day 1 following TBI. Thymuses were harvested 13 days after SL-TBI and cellularity was  
389 assessed and populations were analyzed by flow cytometry.

390

391 **Statistics**

392 All analysis between two groups was performed with a non-parametric Mann-Whitney test.

393 Statistical comparison between 3 or more groups in Figs. 1A, 1C, 1D, 1E, 1F, 1G, 2A, 2B, 2C,

394 2E, 3A, 3H, 3I, and 4A were performed using a one-way ANOVA with Tukey's multiple comparison

395 post-hoc test. All statistics were calculated using Graphpad Prism and display graphs were

396 generated in Graphpad Prism or R.

397

398

399

400

401

402

403

404

405

406

407

408

409

410

411

412

413

414

415

416

417

418

419

420

421 **ACKNOWLEDGEMENTS**

422 We gratefully acknowledge the assistance of the Flow Cytometry and Comparative Medicine Core  
423 Facilities; and the support of the Immunotherapy Integrated Research Center at the Fred  
424 Hutchinson Cancer Research Center. We are grateful to Fionnuala Morrish and Carla Jaeger for  
425 discussions regarding metabolic assays. This research was supported by National Institutes of  
426 Health award numbers R00-CA176376 (J.A.D.), R01-HL145276 (J.A.D.), R01-HL165673  
427 (J.A.D.), U01-AI70035 (J.A.D.), Project 2 of P01-AG052359 (J.A.D.), and the NCI Cancer Center  
428 Support Grant P30-CA015704. Support was also received from a Scholar Award from the  
429 American Society of Hematology (J.A.D.); the Mechtild Harf (John Hansen) Award from the DKMS  
430 Foundation for Giving Life (J.A.D.); the Cuyamaca Foundation (J.A.D.), and the Bezos Family  
431 Foundation (J.A.D.). S.K. was supported by a New Investigator Award from the American Society  
432 for Transplantation and Cellular Therapy and Pilot Funding from the Cooperative Center for  
433 Excellence in Hematology (Fred Hutchinson Cancer Research Center) award number U54  
434 DK106829.

435

436 **AUTHOR CONTRIBUTIONS**

437 S.K. and J.A.D. conceived of the idea of this manuscript. J.A.D., and S.K. designed, analyzed and  
438 interpreted experiments, and drafted the manuscript; C.A.E., K.C., L.I., P.d.R, A.C., K.S.H.,  
439 C.W.S., and D.G. performed experiments; L.S., E.V., and J.A.D. supervised experiments. All  
440 authors contributed to the article and approved the submitted version.

441

442 **CONFLICT OF INTEREST**

443 J.A.D., S.K., and L.I., have submitted a patent application pending around these findings to  
444 promote thymus regeneration.

445

446

447 **REFERENCES**

- 448 1. Kinsella, S. & Dudakov, J.A. When the Damage Is Done: Injury and Repair in Thymus  
449 Function. *Front Immunol* **11**, 1745 (2020).
- 450 2. Chinn, I.K., Blackburn, C.C., Manley, N.R. & Sempowski, G.D. Changes in primary  
451 lymphoid organs with aging. *Semin Immunol* **24**, 309-320 (2012).
- 452 3. Granadier, D., Iovino, L., Kinsella, S. & Dudakov, J.A. Dynamics of thymus function and  
453 T cell receptor repertoire breadth in health and disease. *Semin Immunopathol* **43**, 119-  
454 134 (2021).
- 455 4. van den Broek, T. *et al.* Neonatal thymectomy reveals differentiation and plasticity within  
456 human naive T cells. *The Journal of clinical investigation* **126**, 1126-1136 (2016).
- 457 5. Dudakov, J.A. *et al.* Interleukin-22 Drives Endogenous Thymic Regeneration in Mice.  
458 *Science* **336**, 91-95 (2012).
- 459 6. Goldberg, G.L. *et al.* Sex Steroid Ablation Enhances Immune Reconstitution Following  
460 Cytotoxic Antineoplastic Therapy in Young Mice. *J Immunol* **184**, 6014-6024 (2010).
- 461 7. Gui, J., Mustachio, L.M., Su, D.M. & Craig, R.W. Thymus Size and Age-related Thymic  
462 Involution: Early Programming, Sexual Dimorphism, Progenitors and Stroma. *Aging Dis*  
463 **3**, 280-290 (2012).
- 464 8. Wertheimer, T. *et al.* Production of BMP4 by endothelial cells is crucial for endogenous  
465 thymic regeneration. *Science Immunology* **3** (2018).
- 466 9. Vaidya, H.J., Briones Leon, A. & Blackburn, C.C. FOXN1 in thymus organogenesis and  
467 development. *Eur J Immunol* **46**, 1826-1837 (2016).
- 468 10. Kinsella, S. *et al.* Attenuation of apoptotic cell detection triggers thymic regeneration  
469 after damage. *Cell Rep* **37**, 109789 (2021).
- 470 11. Venereau, E., Ceriotti, C. & Bianchi, M.E. DAMPs from Cell Death to New Life. *Front*  
471 *Immunol* **6**, 422 (2015).
- 472 12. Anders, H.-J. & Schaefer, L. Beyond tissue injury-damage-associated molecular  
473 patterns, toll-like receptors, and inflammasomes also drive regeneration and fibrosis.  
474 *Journal of the American Society of Nephrology : JASN* **25**, 1387-1400 (2014).

487 13. Yang, R. & Tonnesseen, T.I. DAMPs and sterile inflammation in drug hepatotoxicity.  
488 *Hepatol Int* **13**, 42-50 (2019).

489

490 14. Wilgus, T.A. Alerting the body to tissue injury: The role of alarmins and DAMPs in  
491 cutaneous wound healing. *Curr Pathobiol Rep* **6**, 55-60 (2018).

492

493 15. Simader, E. *et al.* Tissue-regenerative potential of the secretome of  $\gamma$ -irradiated  
494 peripheral blood mononuclear cells is mediated via TNFRSF1B-induced necroptosis.  
495 *Cell death & disease* **10**, 729-729 (2019).

496

497 16. Klemm, J., Stinchfield, M.J. & Harris, R.E. Necrosis-induced apoptosis promotes  
498 regeneration in Drosophila wing imaginal discs. *Genetics* **219** (2021).

499

500 17. Cairns, J.S., Mainwaring, M.S., Cacchione, R.N., Walker, J.A. & McCarthy, S.A.  
501 Regulation of apoptosis in thymocytes. *Thymus* **21**, 177-193 (1993).

502

503 18. Yang, Y. & Ashwell, J.D. Thymocyte apoptosis. *J Clin Immunol* **19**, 337-349 (1999).

504

505 19. Erlacher, M. *et al.* Puma cooperates with Bim, the rate-limiting BH3-only protein in cell  
506 death during lymphocyte development, in apoptosis induction. *Journal of Experimental  
507 Medicine* **203**, 2939-2951 (2006).

508

509 20. Erlacher, M. *et al.* BH3-only proteins Puma and Bim are rate-limiting for  $\gamma$ -radiation- and  
510 glucocorticoid-induced apoptosis of lymphoid cells in vivo. *Blood* **106**, 4131-4138 (2005).

511

512 21. Bredenkamp, N., Nowell, C.S. & Blackburn, C.C. Regeneration of the aged thymus by a  
513 single transcription factor. *Development* **141**, 1627-1637 (2014).

514

515 22. Vringer, E. & Tait, S.W.G. Mitochondria and Inflammation: Cell Death Heats Up. *Front  
516 Cell Dev Biol* **7**, 100 (2019).

517

518 23. Jeong, S.Y. & Seol, D.W. The role of mitochondria in apoptosis. *BMB Rep* **41**, 11-22  
519 (2008).

520

521 24. Li, Q. *et al.* The Role of Mitochondria in Pyroptosis. *Front Cell Dev Biol* **8**, 630771  
522 (2020).

523

524 25. Wang, Y. *et al.* Mitochondrial ROS promote macrophage pyroptosis by inducing GSDMD  
525 oxidation. *J Mol Cell Biol* **11**, 1069-1082 (2019).

526

527 26. Zhao, S. *et al.* Reactive Oxygen Species Interact With NLRP3 Inflammasomes and Are  
528 Involved in the Inflammation of Sepsis: From Mechanism to Treatment of Progression.  
529 *Front Physiol* **11**, 571810 (2020).

530

531 27. Pereira, C.A. *et al.* Mitochondrial DNA Promotes NLRP3 Inflammasome Activation and  
532 Contributes to Endothelial Dysfunction and Inflammation in Type 1 Diabetes. *Front  
533 Physiol* **10**, 1557 (2019).

534

535 28. Liu, Q., Zhang, D., Hu, D., Zhou, X. & Zhou, Y. The role of mitochondria in NLRP3  
536 inflammasome activation. *Mol Immunol* **103**, 115-124 (2018).

537

538 29. Mishra, S.R. *et al.* Mitochondrial dysfunction as a driver of NLRP3 inflammasome  
539 activation and its modulation through mitophagy for potential therapeutics. *Int J Biochem  
540 Cell Biol* **136**, 106013 (2021).

541

542 30. Yu, J. *et al.* Inflammasome activation leads to Caspase-1-dependent mitochondrial  
543 damage and block of mitophagy. *Proc Natl Acad Sci U S A* **111**, 15514-15519 (2014).

544

545 31. Bernard, N.J. Mitochondria control pyroptosis. *Nature Immunology* **22**, 1071-1071  
546 (2021).

547

548 32. Boveris, A. & Chance, B. The mitochondrial generation of hydrogen peroxide. General  
549 properties and effect of hyperbaric oxygen. *Biochem J* **134**, 707-716 (1973).

550

551 33. Zhang, H. *et al.* Reduction of elevated proton leak rejuvenates mitochondria in the aged  
552 cardiomyocyte. *Elife* **9** (2020).

553

554 34. Valle-Casuso, J.C., González-Sánchez, A., Medina, J.M. & Tabernero, A. HIF-1 and c-  
555 Src mediate increased glucose uptake induced by endothelin-1 and connexin43 in  
556 astrocytes. *PLoS One* **7**, e32448 (2012).

557

558 35. Zhao, Y. *et al.* Glycogen synthase kinase 3alpha and 3beta mediate a glucose-sensitive  
559 antiapoptotic signaling pathway to stabilize Mcl-1. *Mol Cell Biol* **27**, 4328-4339 (2007).

560

561 36. Chen, C.J. *et al.* Identification of a key pathway required for the sterile inflammatory  
562 response triggered by dying cells. *Nat Med* **13**, 851-856 (2007).

563

564 37. Kuida, K. *et al.* Altered cytokine export and apoptosis in mice deficient in interleukin-1  
565 beta converting enzyme. *Science* **267**, 2000-2003 (1995).

566

567 38. Man, S.M., Karki, R. & Kanneganti, T.D. Molecular mechanisms and functions of  
568 pyroptosis, inflammatory caspases and inflammasomes in infectious diseases. *Immunol  
569 Rev* **277**, 61-75 (2017).

570

571 39. Iovino, L. *et al.* Activation of the zinc-sensing receptor GPR39 promotes T-cell  
572 reconstitution after hematopoietic cell transplant in mice. *Blood* **139**, 3655-3666 (2022).

573

574 40. Dubyak, G.R. & el-Moatassim, C. Signal transduction via P2-purinergic receptors for  
575 extracellular ATP and other nucleotides. *Am J Physiol* **265**, C577-606 (1993).

576

577 41. Abbracchio, M.P. *et al.* International Union of Pharmacology LVIII: update on the P2Y G  
578 protein-coupled nucleotide receptors: from molecular mechanisms and pathophysiology  
579 to therapy. *Pharmacol Rev* **58**, 281-341 (2006).

580

581 42. May, C., Weigl, L., Karel, A. & Hohenegger, M. Extracellular ATP activates ERK1/ERK2  
582 via a metabotropic P2Y1 receptor in a Ca<sup>2+</sup> independent manner in differentiated  
583 human skeletal muscle cells. *Biochemical pharmacology* **71**, 1497-1509 (2006).

584

585 43. Bisaggio, R.D., Nihei, O.K., Persechini, P.M., Savino, W. & Alves, L.A. Characterization  
586 of P2 receptors in thymic epithelial cells. *Cell Mol Biol (Noisy-le-grand)* **47**, 19-31 (2001).

587

588 44. Alves, M., Beamer, E. & Engel, T. The Metabotropic Purinergic P2Y Receptor Family as  
589 Novel Drug Target in Epilepsy. *Front Pharmacol* **9**, 193 (2018).

590

591 45. Gao, F. & Li, X. P2Y11 receptor antagonist NF340 ameliorates inflammation in human  
592 fibroblast-like synoviocytes: An implication in rheumatoid arthritis. *IUBMB Life* **71**, 1552-  
593 1560 (2019).

594

595 46. Feliu, C. *et al.* Complementary Role of P2 and Adenosine Receptors in ATP Induced-  
596 Anti-Apoptotic Effects Against Hypoxic Injury of HUVECs. *Int J Mol Sci* **20** (2019).

597

598 47. Abdulqawi, R. *et al.* P2X3 receptor antagonist (AF-219) in refractory chronic cough: a  
599 randomised, double-blind, placebo-controlled phase 2 study. *Lancet* **385**, 1198-1205  
600 (2015).

601

602 48. Rech, J.C., Bhattacharya, A., Letavic, M.A. & Savall, B.M. The evolution of P2X7  
603 antagonists with a focus on CNS indications. *Bioorg Med Chem Lett* **26**, 3838-3845  
604 (2016).

605

606 49. Keystone, E.C., Wang, M.M., Layton, M., Hollis, S. & McInnes, I.B. Clinical evaluation of  
607 the efficacy of the P2X7 purinergic receptor antagonist AZD9056 on the signs and  
608 symptoms of rheumatoid arthritis in patients with active disease despite treatment with  
609 methotrexate or sulphasalazine. *Ann Rheum Dis* **71**, 1630-1635 (2012).

610

611 50. Sarafoff, N., Byrne, R.A. & Sibbing, D. Clinical use of clopidogrel. *Curr Pharm Des* **18**,  
612 5224-5239 (2012).

613

614 51. Hale, L.P., Braun, R.D., Gwinn, W.M., Greer, P.K. & Dewhirst, M.W. Hypoxia in the  
615 thymus: role of oxygen tension in thymocyte survival. *Am J Physiol Heart Circ Physiol*  
616 **282**, H1467-1477 (2002).

617

618 52. Braun, R.D., Lanzen, J.L., Snyder, S.A. & Dewhirst, M.W. Comparison of tumor and  
619 normal tissue oxygen tension measurements using OxyLite or microelectrodes in  
620 rodents. *Am J Physiol Heart Circ Physiol* **280**, H2533-2544 (2001).

621

622 53. Sun, V. *et al.* The Metabolic Landscape of Thymic T Cell Development In Vivo and In  
623 Vitro. *Front Immunol* **12**, 716661 (2021).

624

625 54. Sanman, L.E. *et al.* Disruption of glycolytic flux is a signal for inflammasome signaling  
626 and pyroptotic cell death. *Elife* **5**, e13663 (2016).

627

628 55. Barnstable, C.J., Reddy, R., Li, H. & Horvath, T.L. Mitochondrial Uncoupling Protein 2  
629 (UCP2) Regulates Retinal Ganglion Cell Number and Survival. *J Mol Neurosci* **58**, 461-  
630 469 (2016).

631

632 56. Miao, Y. *et al.* Increasing UCP2 expression and decreasing NOX1/4 expression maintain  
633 chondrocyte phenotype by reducing reactive oxygen species production. *Oncotarget* **8**,  
634 63750-63763 (2017).

635

636 57. Bach, D. *et al.* Mitofusin-2 determines mitochondrial network architecture and  
637 mitochondrial metabolism. A novel regulatory mechanism altered in obesity. *J Biol Chem*  
638 **278**, 17190-17197 (2003).

639

640 58. Minutoli, L. *et al.* ROS-Mediated NLRP3 Inflammasome Activation in Brain, Heart,  
641 Kidney, and Testis Ischemia/Reperfusion Injury. *Oxid Med Cell Longev* **2016**, 2183026  
642 (2016).

643

644 59. Pétrilli, V. *et al.* Activation of the NALP3 inflammasome is triggered by low intracellular  
645 potassium concentration. *Cell Death Differ* **14**, 1583-1589 (2007).

646

647 60. Dostert, C. *et al.* Innate immune activation through Nalp3 inflammasome sensing of  
648 asbestos and silica. *Science* **320**, 674-677 (2008).

649

650 61. Tschopp, J. & Schroder, K. NLRP3 inflammasome activation: The convergence of  
651 multiple signalling pathways on ROS production? *Nat Rev Immunol* **10**, 210-215 (2010).

652

653 62. Heid, M.E. *et al.* Mitochondrial reactive oxygen species induces NLRP3-dependent  
654 lysosomal damage and inflammasome activation. *J Immunol* **191**, 5230-5238 (2013).

655

656 63. Howard, J.D., Sarojini, H., Wan, R. & Chien, S. Rapid granulation tissue regeneration by  
657 intracellular ATP delivery--a comparison with Regranex. *PLoS One* **9**, e91787 (2014).

658

659 64. Sarojini, H. *et al.* Rapid tissue regeneration induced by intracellular ATP delivery-A  
660 preliminary mechanistic study. *PLoS One* **12**, e0174899 (2017).

661

662 65. Hill, L.M., Gavala, M.L., Lenertz, L.Y. & Bertics, P.J. Extracellular ATP may contribute to  
663 tissue repair by rapidly stimulating purinergic receptor X7-dependent vascular  
664 endothelial growth factor release from primary human monocytes. *J Immunol* **185**, 3028-  
665 3034 (2010).

666

667 66. McEwan, T.B. *et al.* Autocrine regulation of wound healing by ATP release and P2Y(2)  
668 receptor activation. *Life Sci* **283**, 119850 (2021).

669

670 67. Gendaszewska-Darmach, E. & Kucharska, M. Nucleotide receptors as targets in the  
671 pharmacological enhancement of dermal wound healing. *Purinergic Signalling* **7**, 193  
672 (2011).

673

674 68. Greig, A.V., James, S.E., McGrouther, D.A., Terenghi, G. & Burnstock, G. Purinergic  
675 receptor expression in the regeneration epidermis in a rat model of normal and delayed  
676 wound healing. *Exp Dermatol* **12**, 860-871 (2003).

677

678 69. Shahidullah, M. & Wilson, W.S. Mobilisation of intracellular calcium by P2Y2 receptors in  
679 cultured, non-transformed bovine ciliary epithelial cells. *Curr Eye Res* **16**, 1006-1016  
680 (1997).

681

682 70. Boucher, I., Rich, C., Lee, A., Marcincin, M. & Trinkaus-Randall, V. The P2Y2 receptor  
683 mediates the epithelial injury response and cell migration. *Am J Physiol Cell Physiol* **299**,  
684 C411-421 (2010).

685

686 71. Mai, Y. *et al.* P2X Receptors: Potential Therapeutic Targets for Symptoms Associated  
687 With Lung Cancer - A Mini Review. *Front Oncol* **11**, 691956 (2021).

688

689 72. Lau, O.C., Samarawickrama, C. & Skalicky, S.E. P2Y2 receptor agonists for the  
690 treatment of dry eye disease: a review. *Clin Ophthalmol* **8**, 327-334 (2014).

691

692 73. Pernes, G., Flynn, M.C., Lancaster, G.I. & Murphy, A.J. Fat for fuel: lipid metabolism in  
693 haematopoiesis. *Clin Transl Immunology* **8**, e1098 (2019).

694

695 74. Velardi, E. et al. Sex steroid blockade enhances thymopoiesis by modulating Notch  
696 signaling. *The Journal of Experimental Medicine* **211**, 2341-2349 (2014).

697

698

699 **FIGURE LEGENDS**

700 **Figure 1: A switch from apoptotic to pyroptotic DP thymocytes triggers thymus**  
701 **regeneration. A-E**, Thymus was analyzed from 6-8 week old C57/BL/6 mice at days 0,1 2, 3 and  
702 7 following sublethal total body irradiation (TBI, 550cGy). **A**, Total thymic cellularity and proportion  
703 of cellularity as a function of baseline cellularity (n=15-19/timepoint from 5 independent  
704 experiments). **B**, Concatenated flow cytometry plot of CD4 vs CD8 (gated on viable CD45+ cells)  
705 (n=9-13 from 3-4 independent experiments). **C**, Concatenated flow cytometry plot from one  
706 experiment showing cleaved caspase-3 on DP thymocytes (Gated on CD45+CD4+CD8+ cells)  
707 and bar graph showing proportion of cleaved-cas3+ DP thymocytes (n=15-16/timepoint from 5  
708 independent experiments). **D**, Concatenated flow cytometry plot from one experiment showing  
709 cleaved-caspase1 and PI (gated on CD45+CD4+CD8+ cells) and bar graph with proportions  
710 (n=13/timepoint from 4 independent experiments). **E**, Magnitude of change in expression of  
711 cleaved-caspase-1 and cleaved-caspase-3 in DP thymocytes after TBI. (n=10-  
712 15/timepoint/condition from 4-5 independent experiments). **F**, Lactate dehydrogenase levels were  
713 measured in the thymus supernatant of mice (n=4 mice/group). **G**, Gasdermin D levels were  
714 measured in CD45+ cells from the thymus at days 0,1 2, 3, 7, and 14 post TBI (n=3-4 mice/group  
715 from 2-3 independent experiments). **H**; Cells were co-cultured with freshly isolated thymocytes  
716 treated to induce or inhibit pyroptosis and Foxn1 expression was measured by qPCR, 20 h after  
717 co-culture, in 1C9s (n =8-11 thymuses from 3 separate experiments), ANV42.1 (n=8 thymuses

718 from 3 separate experiments), and TE-71 (n=11 from 3 separate experiments). Data represents  
719 mean  $\pm$  SEM.

720

721 **Figure 2: Dysregulated metabolism redirects pyruvate to fuel OXPHOS in thymocytes after**  
722 **damage. A-F**, Mitochondrial function was analyzed in the thymus isolated from 6-8 week old  
723 C57/BL/6 mice at days 0, 1, 2, 3 and 7 following sublethal total body irradiation (TBI, 550cGy). **A**,  
724 Mitochondrial membrane potential assessed by staining of TMRE. Concatenated histogram of  
725 TMRE on DP thymocytes (left), quantification of TMRE+ proportions (right) (n=8-12 mice from 3  
726 separate experiments). **B**, Correlation of TMRE expression with Caspase-1 MFI (n=3-8 from 3  
727 independent experiments). **C**, Mitochondrial mass assessed by Mitotracker Green. Concatenated  
728 histogram of TMRE on DP thymocytes (left), quantification of TMRE+ proportions (right) (n=9-10  
729 mice from 3 independent experiments). **D**, Correlation of TMRE expression with Caspase-1 MFI  
730 (n=6/timepoint from 3 independent experiments). **E**, Mitochondrial ROS was assessed by staining  
731 for MitoSOX. Concatenated histogram of TMRE on DP thymocytes (left), quantification of TMRE+  
732 proportions (right) (n=5-7 mice from 2 separate experiments). **F**, Correlation of TMRE expression  
733 with Caspase-1 MFI (n=5-7/timepoint from 2 independent experiments). **G**, RNA seq was carried  
734 out on FACS purified CD4+CD8+ thymocytes from untreated and TBI-treated (1 day post TBI)  
735 mice (n=3/group). Displayed are heatmaps for expression of key genes involved with OXPHOS  
736 and glycolysis. **H**, Intracellular lactate and pyruvate levels were measured in freshly isolated  
737 thymocytes from untreated and TBI-treated mice (n=5 mice/group from 2 separate experiments).  
738 **I-K**, Thymocytes isolated from mice at days 0 or 1 post TBI were incubated with RPMI  
739 supplemented with pyruvate (5 mM) for 4 h. **I**, Concatenated histogram showing expression of  
740 cleaved-caspase-1 on DP thymocytes in cells incubated with media alone, high pyruvate (on  
741 day 0 thymocytes) or normal media with thymocytes isolated at d1 following TBI. **J**, Proportion of  
742 Cleaved-caspase-1+GhostDye+ cells (n=6 mice from 2 separate experiments). **K**, Proportion of  
743 mitoSOX+ DP thymocytes (n=6 mice from 2 separate experiments). **L**, Freshly isolated

744 thymocytes from untreated mice were incubated with RPMI supplemented with pyruvate (5 mM)  
745 for 4 h plus TEMPOL (100  $\mu$ M). cl-caspase 1 levels were measured using flow cytometry (n=6  
746 mice from 2 separate experiments). **M**, Freshly isolated thymocytes from untreated mice were  
747 incubated with RPMI supplemented with pyruvate (5 mM) for 4 h plus  $\alpha$ -ketobutyrate (200  $\mu$ M).  
748 cl-caspase 1 levels were measured using flow cytometry (n=13-14 mice from 4 separate  
749 experiments). Data represents mean  $\pm$  SEM.

750

751 **Figure 3: Activation of the P2Y2 receptor with extracellular ATP induces FOXN1 in cTECs.**  
752 **A**, The cTEC cells line 1C9 was treated with a panel of DAMPs and *Foxn1* transcription was  
753 measured in by qPCR 20 h following incubation (n=3-4 separate experiments). **B**, A second  
754 cTEC cell line (ANV42.1) was treated with ATP (100  $\mu$ M) and *Foxn1* expression was measured  
755 after 20 h (n=3 separate experiments). **C**, Freshly isolated human cTECs were treated with ATP  
756 (100  $\mu$ M) and *Foxn1* expression was measured after 20 h (n= 2). **D**, cTECs, MHCII<sup>hi</sup> mTEC, and  
757 MHCII<sup>lo</sup> mTEC were isolated from untreated 6wo C57BL/6 mice and RNA sequencing performed.  
758 Displayed is expression of purinergic receptor family members (n=3/cell population). **E**, Purinergic  
759 receptor expression in FACS purified cTECs from untreated mice measured by qPCR (n=2-3  
760 pooled mouse thymuses). **F**, Intracellular free  $\text{Ca}^{2+}$  levels were measured by flow cytometry in  
761 untreated and TBI-treated (day 4 post TBI) cTECs (n=10 mice from 2 separate experiments) and  
762 mTECs (n=8-10 mice from 2 separate experiments). **G**, Correlation of free  $\text{Ca}^{2+}$  and *Foxn1*  
763 expression at days 0 and 4 after SL-TBI (n=3/timepoint). **H**, 1C9 (cTEC) were treated with  
764 tunicamycin (1  $\mu$ M) or thapsigargin (100 nM) for 20 h and *Foxn1* expression was measured by  
765 qPCR (n=4 independent experiments). **I**, 1C9 (cTECs) were treated with ATP and either  
766 antagonists for P2Y2 or P2X4 and *Foxn1* expression was measured by qPCR 20 h after  
767 incubation (n=5 separate experiments). Data represents mean  $\pm$  SEM.

768

769 **Figure 4: Activation of the P2Y2 enhances thymus regeneration after damage. A, ANV42.1**  
770 (cTEC) cells were treated with the P2Y2 agonist UTPyS and the P2Y2 antagonist ARC-118925XX  
771 for 20 h and *Foxn1* expression was measured by qPCR after 20 h (n=3 separate experiments);  
772 **B-D**, 6wo C57BL/6 mice were treated with UTPyS (1 mg/kg) IP at day 1 following SL-TBI and the  
773 thymuses were harvested at day 13. **B**, Total thymus cellularity. **C**, Number of CD4-CD8- double  
774 negative (DN), DP, of CD4 or CD8+ single positive (SP4 or SP8, respectively) thymocytes (n=23-  
775 24 mice from 3 independent experiments). Data represents mean  $\pm$  SEM.

776 **Supplementary Figure 1**

777 Thymuses from 6-8 week old C57BL/6 mice were harvested at days 0, 1, 2, 3 and 7 following TBI  
778 and glutathione levels were measured by flow cytometry in DP thymocytes (n=3 mice).

779

780

781

782

783

784

785

786

787

788

789

790

791

792

793

794

## Figure 1

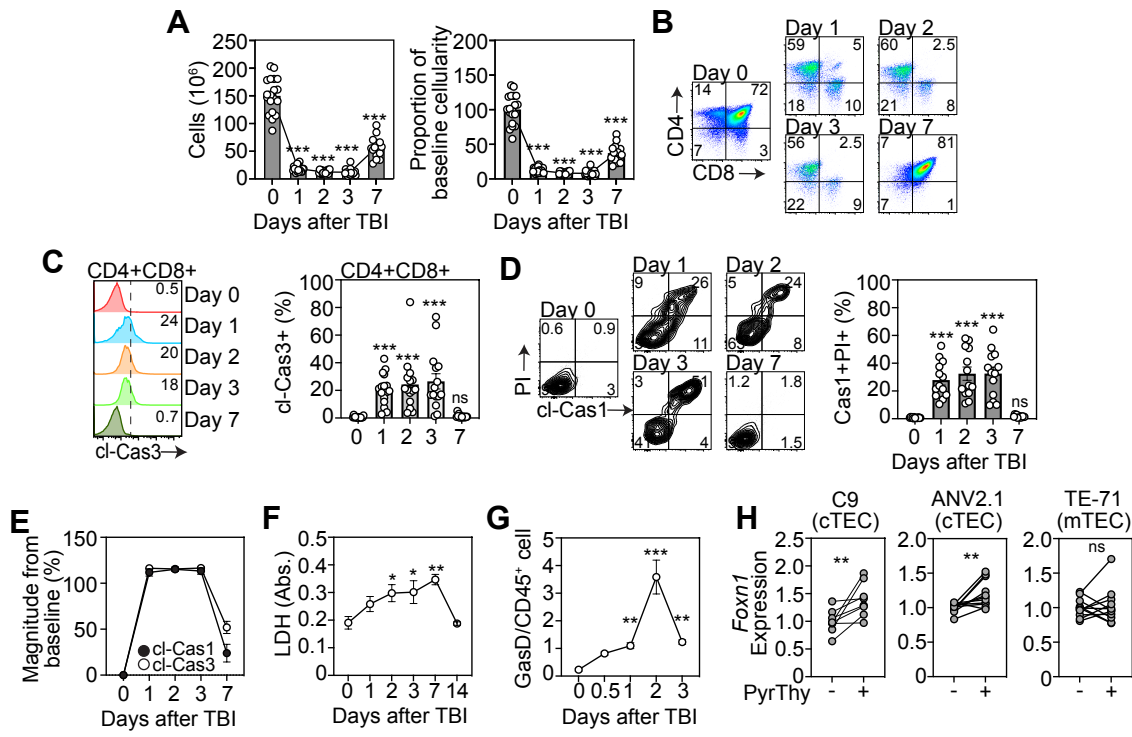


## Figure 2

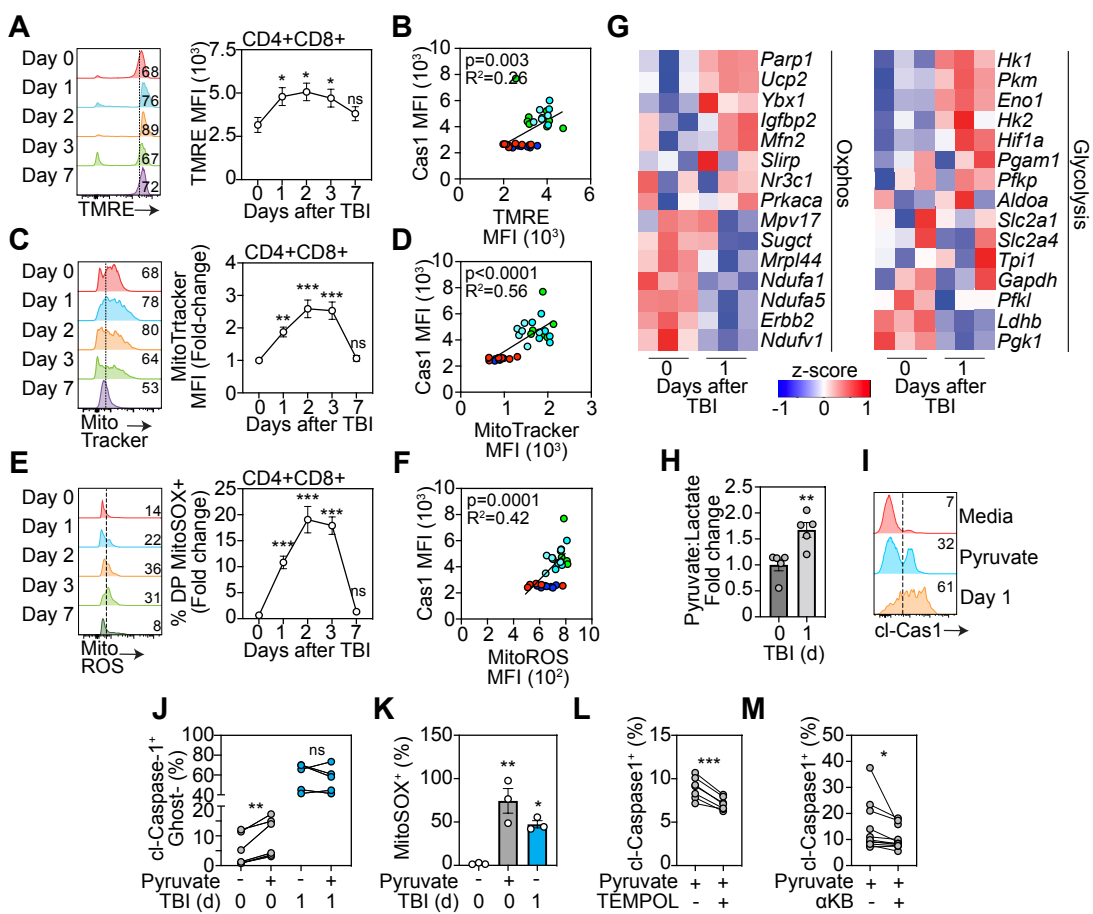


**Figure 3**

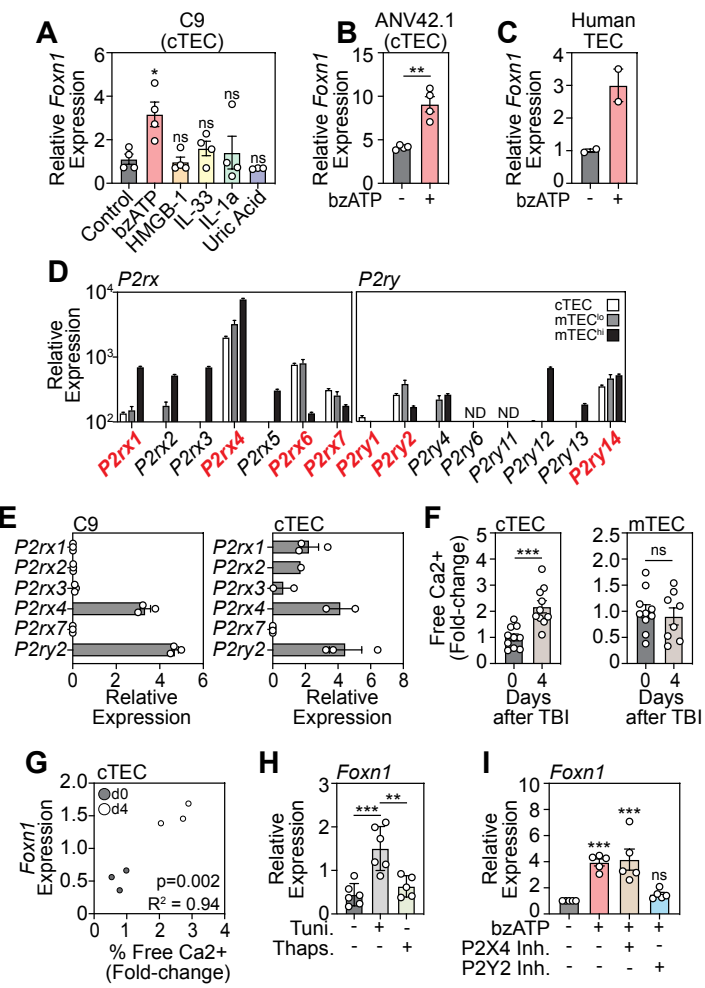


**Figure 4**

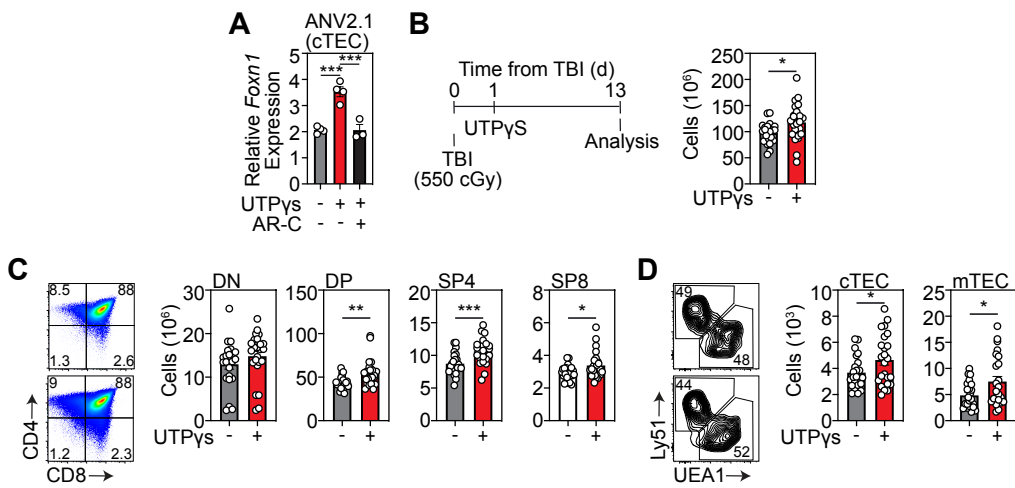


## Figure S1

